Sensitive Detection of Carcinoembryonic Antigen Using Stability-Limited Few-Layer Black Phosphorus as an Electron Donor and a Reservoir

*Jian Peng, Youqun Lai, Yuanyuan Chen, Jun Xu, Liping Sun, and Jian Weng**

The instability of few-layer black phosphorus (FL-BP) hampers its further applications. Here, it can be demonstrated that the instability of FL-BP can also be the advantage for application in biosensor. First, gold nanoparticle/FL-BP (BP-Au) hybrid is facilely synthesized by mixing Au precursor with FL-BP. BP-Au shows outstanding catalytic activity ($K = 1120\ s^{-1}\ g^{-1}$) and low activation energy ($17.53\ kJ\ mol^{-1}$) for reducing 4-nitrophenol, which is attributed to the electron-reservoir and electron-donor properties of FL-BP, and synergistic interaction of Au nanoparticles and FL-BP. Oxidation of FL-BP after catalytic reaction is further confirmed by transmission electron microscope, X-ray photoelectron spectroscopy, and zeta potentials. Second, the catalytic activity of BP-Au can be reversibly switched from "inactive" to "active" upon treatment with antibody and antigen in solution, thus providing a versatile platform for label-free colorimetric detection of biomarkers. The sensor shows a wide detection range ($1\ pg\ mL^{-1}$ to $-10\ \mu g\ mL^{-1}$), high sensitivity ($0.20\ pg\ mL^{-1}$), and selectivity for detecting carcinoembryonic antigen (CEA). Finally, the biosensor has been used to detect CEA in colon and breast cancer clinical samples with satisfactory results. Therefore, the instability of BP can also be the advantage for application in detecting cancer biomarker in clinic.

1. Introduction

Phosphorus has three main allotropes, including white phosphorus, red phosphorus, and black phosphorus (BP).[1] BP is a layered semiconductor that consists of corrugated planes of phosphorus atoms with strong in-plane covalent bonding and weak interlayer van der Waals interactions. 2D BP, also named as single-layer or few-layer black phosphorus (FL-BP), has received a great deal of attention over the last 2 years.[2] Unlike graphene, FL-BP is a semiconductor with a thickness-dependent, direct band gap ranging from ≈0.3 eV in the bulk to ≈1.5 eV in the monolayer phosphorene.[3] Compared with molybdenum disulfide, FL-BP has a higher mobility (≈200–1000 $cm^2\ V^{-1}\ s^{-1}$), larger on/off ratio (>10^5), and anisotropic properties.[4] These fascinating properties suggest that FL-BP is not only promising in nanoscale electronic devices, but also suitable for the development of energy storage, and optoelectronic and molecular sensing applications.[1,4a,b,5] Although BP is the most thermodynamically stable allotrope of phosphorus, it is also very reactive to oxygen, water, and light under ambient conditions, resulting in compositional and physical changes and consequently considerable degradation in the electronic and optical properties.[6] Thus, the lack of air and water stability hampers its further applications in electronic and optical devices. Several methods, including

Dr. J. Peng, Y. Y. Chen, Dr. L. P. Sun, Prof. J. Weng
College of Materials
Xiamen University
Xiamen 361005, P. R. China
E-mail: jweng@xmu.edu.cn
Y. Q. Lai
Department of Radiation Oncology
The First Affiliated Hospital of Xiamen University
Xiamen 361003, P. R. China
Dr. J. Xu, Dr. L. P. Sun, Prof. J. Weng
Research Institute for Biomimetics and Soft Matter
Xiamen University
Xiamen 361005, P. R. China

DOI: 10.1002/smll.201603589

aryl diazonium covalent functionalization, titanium sulfonate ligand surface coordination, organic molecule capping, and Al_2O_3 coating, have been adopted to improve its stability for constructing optoelectronic devices.[4b,7] However, there is no report on the application of stability-related limitation of FL-BP.

The easy degradation of BP in air means strong reducibility and excellent electron-donor capacity. The densities of state calculated by density functional theory of both the bulk structure and a single monolayer of BP exhibit narrow band gaps with widths of 0.2 and 0.51 eV, and low potentials with values of + 0.21 and 0.48 V, respectively.[8] The low redox potential indicates that BP can serve as an electron donor to provide electrons. At the same time, some results have demonstrated that BP has excellent electron-transfer properties.[8,9] We can imagine that the good electron-donor capacity and excellent electron-transfer properties of BP will enhance the reducibility of catalyst in a redox reaction, which can be used to improve the sensitivity of a biosensor. Thus, the stability-related limitation of BP can also be the advantage for application in the biosensor. At the same time, the lone pair electrons of FL-BP, as an electron reservoir, can readily react with oxygen to form phosphite ion, phosphate ion, and other P_xO_y species with nontoxic intermediates, which enable higher biocompatibility and health safety.[2b,10] Phosphorus is an essential element for maintaining good health in humans as phosphates are a component of DNA, RNA, adenosine triphosphate, and also the phospholipids that form all cell membranes, thus showing good biocompatibility and potential application in biomedical field.[11,12]

Herein, Au nanoparticle (NP)-decorated FL-BP (BP-Au), prepared by mixing hexachloroauric acid ($HAuCl_4$) with FL-BP in water (**Scheme 1**a), demonstrates high catalytic activity for 4-nitrophenol (4-NP) reduction. This reaction offers a colorimetric signal output from yellow 4-NP to colorless 4-aminophenol (4-AP), which is used to detect cancer biomarker in clinical samples (Scheme 1b). At the same time, BP is oxidized and provides electrons to accelerate 4-NP reduction. Then, upon addition of carcinoembryonic antibody (anti-CEA), the catalytic activity of BP-Au is "switched off" resulting from adsorption of anti-CEA onto Au surface to inhibit the activity of catalyst. Finally, added carcinoembryonic antigen (CEA) will bind with anti-CEA to form antigen–antibody complex in solution, shifting the equilibrium to desorb the anti-CEA from the surface of BP-Au, when, in turn, the catalytic reaction is "switched on" (Scheme 1b). FL-BP with high electron-transfer capacity and excellent electron-donor capacity greatly improves the catalytic activity toward reducing 4-NP, thus improving the detection sensitivity for cancer biomarker. At last, a highly sensitive and selective colorimetric method for CEA detection is developed and used to detect CEA in clinical samples of colon and breast cancer patients.

2. Results and Discussion

2.1. Preparation and Characterization of BP-Au

2.1.1. Preparation and Characterization of FL-BP

In this study, bulk BP was prepared from red phosphorus by a facile low-pressure transport route and characterized well (see Section 1.2 and Figure S1 in the Supporting Information).[13] To produce FL-BP, polyvinylpyrrolidone (PVP)-assisted liquid-phase exfoliation was adopted. Compared with exfoliating bulk BP in water to prepare FL-BP (FL-BP/H_2O), exfoliating bulk BP in PVP to prepare FL-BP has a higher yield (33.4% vs 6.2%; Figure S2, Supporting Information), which is also higher than other reports.[14] The pyrrolidinone group of PVP, which is also contained in *N*-methyl-2-pyrrolidone and *N*-cyclohexyl-2-pyrrolidone, contributed to the high yield.[7d,14a] The optimal PVP concentration and sonication time are 0.5 mg mL^{-1} and 20 h, respectively (Figure S2, Supporting Information). X-ray photoelectron spectroscopy (XPS) spectra and transmission electron microscope (TEM) images indicate that the as-prepared FL-BP is slowly oxidized compared to FL-BP/H_2O (Figure S3, Supporting Information). The scanning electron microscope (SEM) image shows that the diameter of FL-BP is several hundred nanometers

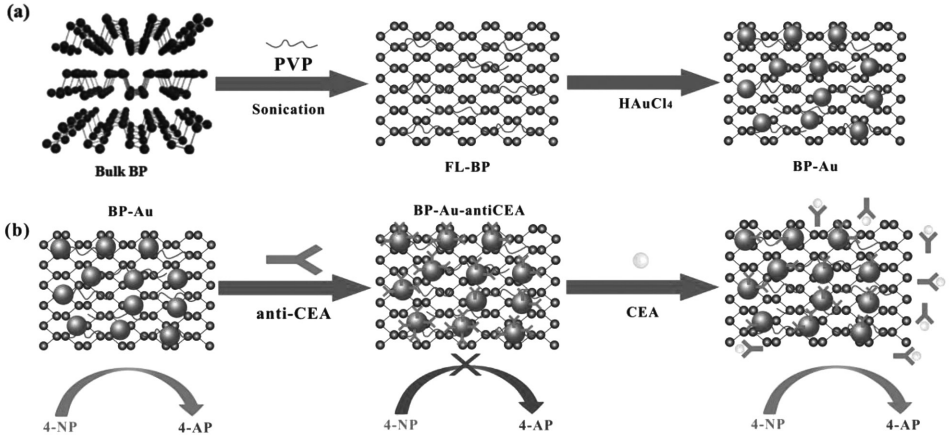

Scheme 1. a) Schematic of exfoliating bulk BP into FL-BP in polyvinylpyrrolidone (PVP) solution and preparing BP-Au hybrid. Bulk BP was exfoliated in PVP solution and FL-BP was stabilized efficiently by PVP. FL-BP served as a reducing agent and platform for Au NPs to grow uniformly. b) Schematic of colorimetric immunological detection of CEA based on the catalytic reduction 4-nitrophenol (4-NP) by BP-Au.

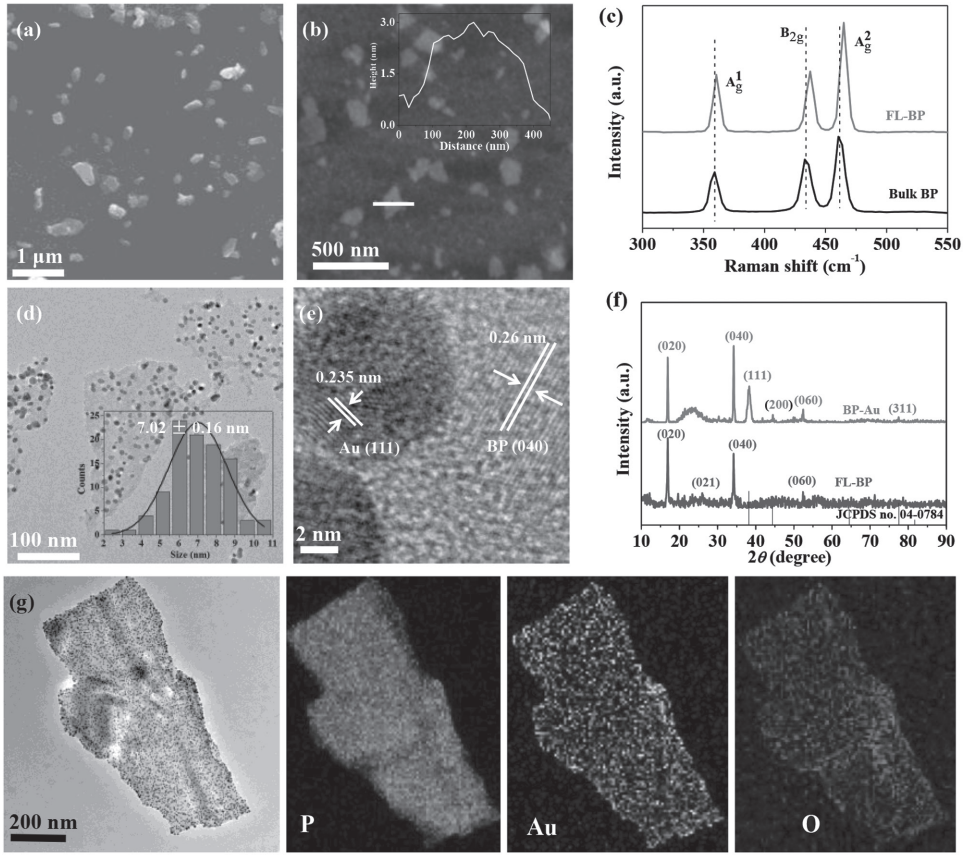

Figure 1. a) SEM of FL-BP. b) AFM of FL-BP and height profile (inset) along the white line. c) Raman spectra of FL-BP and bulk BP. d) TEM image of BP-Au hybrid. Inset: Corresponding particle size distribution obtained by statistical analysis over 100 particles. e) HRTEM image of BP-Au hybrid. f) XRD patterns of FL-BP and BP-Au hybrid. g) TEM image along with elemental maps of P, Au, and O for an individual BP-Au hybrid.

(**Figure 1**a). Atomic force microscope (AFM) shows that the thickness of FL-BP is 2–3 nm (Figure 1b), which is about five individual phosphorene layers.[9a] Raman spectra of bulk BP and FL-BP (Figure 1c) indicate that FL-BP maintains the structure of bulk BP, which is further supported by the X-ray diffraction (XRD) pattern of FL-BP (Figure 1f). Compared with bulk BP, the Raman spectrum of FL-BP shows slightly shift toward high wavenumber, ascribing to the ultrathin thickness of the nanosheets.[2a] High-resolution TEM (HRTEM) image of FL-BP indicates the hexagonal lattice structure for FL-BP with a lattice spacing of 0.26 nm indexed to the (040) plane of BP (Figure S4, Supporting Information). The high-angle annular dark field-scanning transmission electron microscopy (HAADF-STEM) images of FL-BP in Figure S5 (Supporting Information) indicate the uniform distribution of P and O over whole nanosheet, confirming the successful production of FL-BP. The zeta potentials of FL-BP and FL-BP/H_2O are –26.1 and –47.8 mV, respectively (Figure S6, Supporting Information), further confirming that the oxidation of FL-BP can be decreased when bulk BP is exfoliated in PVP.

2.1.2. Preparation and Characterization of BP-Au

When a piece of bulk BP was immersed in $HAuCl_4$ solution, it could react with $HAuCl_4$ to produce Au NPs. The surface of bulk BP was oxidized and became golden yellow (Figure S7c, inset, Supporting Information). Spontaneously reducing $HAuCl_4$ and decorating Au NPs on the surface of bulk BP were observed (Figure S7c,d, Supporting Information). Notably, Au NPs were uniformly decorated on the base plane of bulk BP. Similarly, after mixing FL-BP with $HAuCl_4$ solution in ambient environments (Figure S8, Supporting Information), the color of the solution was changed from brown to purple and an obvious peak at 545 nm in UV–vis spectrum is observed, attributing to the typical surface plasmon resonance absorption of Au NPs. TEM image (Figure 1d) shows that Au NPs are uniformly dispersed on the surface of FL-BP and the size is about 7.02 nm (Figure 1d, inset). Figure 1e shows the hexagonal lattice structure with the lattice spacings of 0.235 and 0.26 nm indexed to (111) plane of face-centered cubic (fcc) Au NPs (JCPDS card NO: 04-0784) and the (040) plane of BP, respectively. XRD patterns further supported that Au NPs had grown on FL-BP (Figure 1f). Figure 1g shows the HAADF-STEM image of BP-Au hybrid, indicating the uniform distribution of P, O, and Au elements in the BP-Au nanosheet. XPS further supports that FL-BP would spontaneously reduce $AuCl_4^-$ (**Figure 2**). Full-scan XPS spectrum (Figure 2a) suggests that the BP-Au hybrid mainly contains three elements, P, Au, and O. Compared to a weak peak at 133 eV from FL-BP (Figure S3b, Supporting Information), an obvious peak at 134.5 eV in BP-Au (Figure 2b) is assigned to P_xO_y,

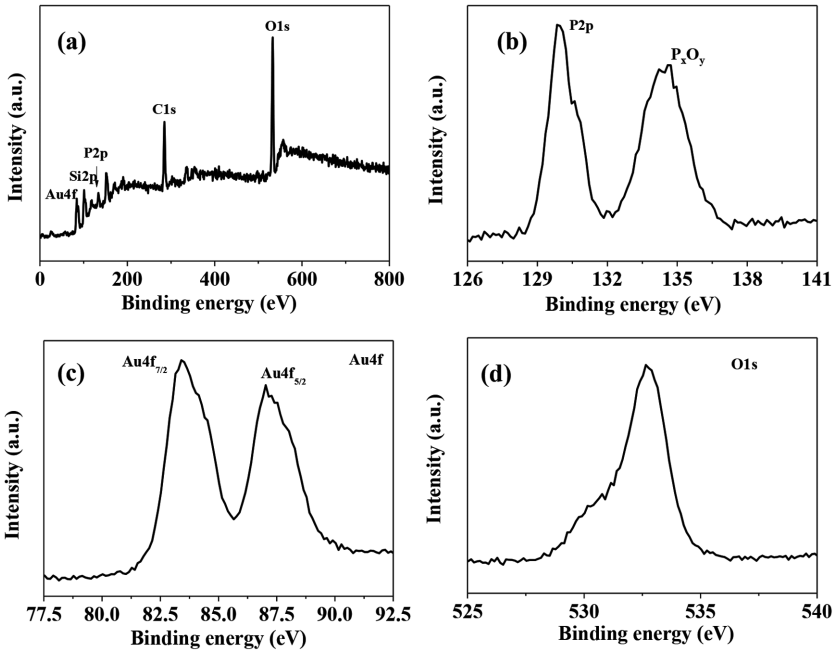

Figure 2. XPS spectra of BP-Au. a) Full XPS spectrum of the as-synthesized BP-Au. High-resolution XPS spectra of b) P 2p peaks, c) Au 4f peaks, and d) O 1s peak of BP-Au.

indicating the further oxidation of FL-BP during reducing $HAuCl_4$ to produce Au NPs, which is further supported by the energy-dispersive X-ray (EDX) spectra (Figure S9, Supporting Information) and the decrease of zeta potential from –26.1 to –40.0 mV (Figure S10, Supporting Information). The Au 4f doublet, Au $4f_{7/2}$, and Au $4f_{5/2}$, were observed at 83.6 and 87.4 eV (Figure 2c), suggesting the existence of Au^0.[15] Figure S11 (Supporting Information) shows TEM images of BP-Au prepared at different reaction times, and 5 min is the optimal reaction time to produce BP-Au. Control experiments (Figure S12, Supporting Information) indicate bare FL-BP/H_2O itself could reduce $HAuCl_4$ to produce Au NPs without other stabilizer or reducing agent.

The underlying mechanism is likely due to the redox reaction between FL-BP and gold ions. The work function of FL-BP is thickness dependent ranging from 5.16 eV for monolayer BP, 4.5 eV for five layers to 4.71 eV for bulk BP, situating the Fermi level of BP well above the reduction potential of $AuCl_4^-$ (+1.002 V vs the standard hydrogen electrode; Figure S13, Supporting Information).[11,16] Therefore, FL-BP/$AuCl_4^-$ could form a redox pair, allowing spontaneous electron transfer from FL-BP to gold ions to occur, and leading to the formation of Au NPs. The similar result was also reported that the deposition of Au NPs on the reduced graphene oxide (RGO) was achieved without the assistance of any reducing agents.[17] The result was attributed to the edge defects (–OH, –COOH, etc.) in RGO introduced by HNO_3 treatment. Both chemically modified graphene and few-layer BP possess ambipolar conduction type which may contribute to this reduction of $HAuCl_4$. Furthermore, FL-BP could also reduce silver nitrate to produce silver nanoparticles (Figure S14, Supporting Information). Therefore, the instability, especially reducibility, of FL-BP could be used to prepare BP–noble metal hybrids.

2.2. Application of BP-Au

2.2.1. Catalytic Activity of BP-Au toward 4-NP Reduction

To investigate catalytic activity of BP-Au, reducing 4-NP to 4-AP in the presence of excess amount of $NaBH_4$ was chosen as the model reaction. The yellow solution of 4-NP and $NaBH_4$ mixture had a clear UV–vis absorption peak at 400 nm. Absorption signal remained unchanged if no other action was taken. However, the yellow mixture rapidly faded and ultimately bleached in quick succession once a small amount of BP-Au (0.01 mg) was added (**Figure 3**a, inset). The reaction was clearly monitored by time-dependent UV–vis absorption spectra. As shown in Figure 3a, the peak at 400 nm disappeared; while a new peak at 300 nm, which was a characteristic absorption of reduction product 4-AP, appeared gradually, indicating the reduction of 4-NP catalyzed by BP-Au. The relationship between $\ln(C_t/C_0)$ and time (t) revealed a linear correlation ($\ln(C_t/C_0) = -11.2 \times 10^{-3}\ t + 0.0534$, $R^2 = 0.9943$). C_0 and C_t are the concentrations of 4-NP at reaction times of 0 and t, respectively. Based on the gradient, the calculated rate constant (k) was 11.2×10^{-3} s^{-1} (Figure 3b). In order to compare the catalytic efficiency with other catalyst, the activity factor K is taken into account, according to the definition, $K = k/m$ where k stands for rate constant and m refers to total mass of the catalyst. The activity factor K of BP-Au was 11.2×10^{-3} s^{-1}/(0.01 mg) = 1120 s^{-1} g^{-1}, which is 3.86 times higher than that of Au NPs loaded with reduced graphene oxide (RGO-Au), and much higher than that of other catalysts (Table S1, Supporting Information). Furthermore, thermodynamics of 4-NP reduction catalyzed by BP-Au was further investigated at different temperatures from 30 to 50 °C (Figure S15, Supporting Information). The calculated activation energy E_a (17.53 kJ mol^{-1}) is lower than that of other reported catalysts (Table S2, Supporting Information). Therefore, these results show that BP-Au has a higher catalytic activity.

Catalytic activity of BP-Au may be influenced by the size and the loading amount of Au NPs that can be tuned by adjusting $HAuCl_4$ concentration (Figure 3c). When $HAuCl_4$ concentration is low (0.05×10^{-3} M), particles size is relatively larger (7.96 nm) and the loading amount (2.9%) is low (Figures S16a,b and S17, Supporting Information), thus resulting in a relatively low catalytic activity ($k = 4.9 \times 10^{-3}$ s^{-1}). When $HAuCl_4$ concentration is high (0.20×10^{-3} M), FL-BP nanosheets are excessively oxidized so that no intact nanosheet can be observed and the size of Au NPs is relatively larger (9.78 nm; Figures S16e,f and S17, Supporting Information), thus resulting in medium catalytic activity ($k = 7.1 \times 10^{-3}$ s^{-1}) even though loading amount is as high as 11.6%. However, when $HAuCl_4$ concentration (0.1×10^{-3} M) and the loading amount (7.2%) are the medium

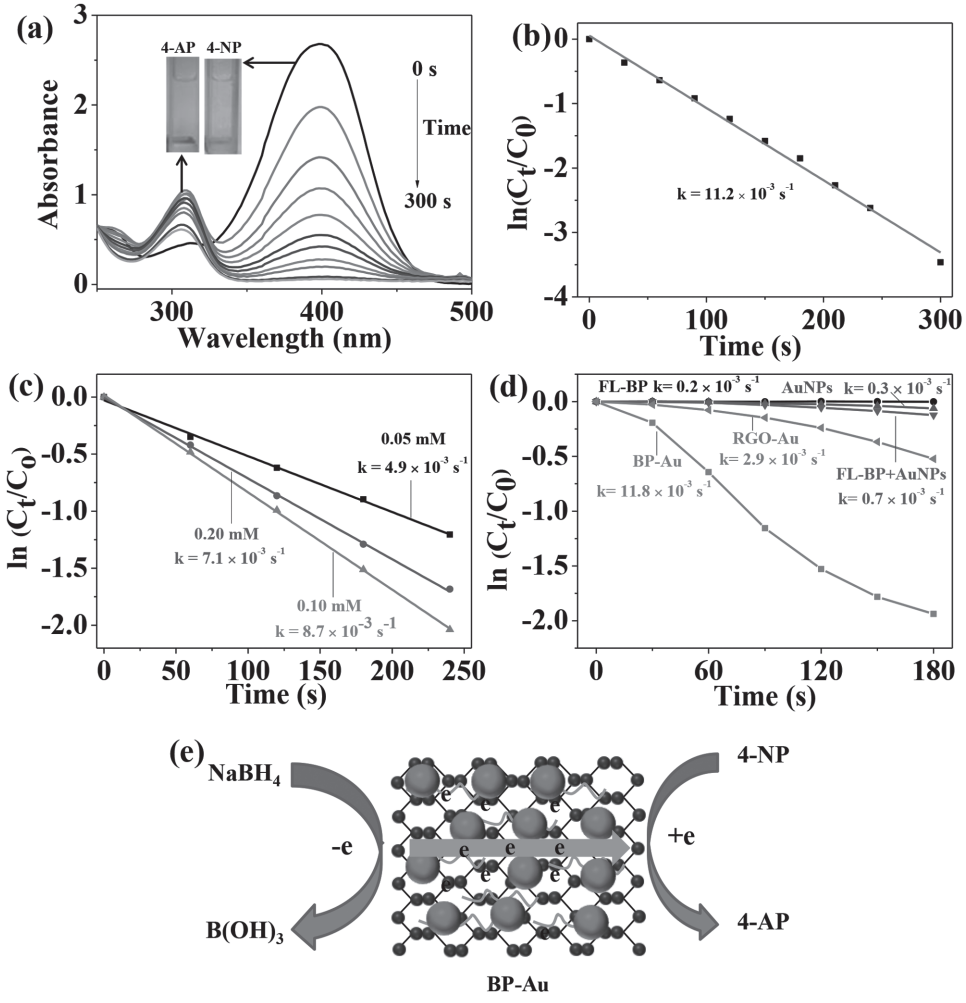

Figure 3. a) UV–vis absorption spectra of 4-NP reduced by $NaBH_4$ in the presence of BP-Au from 0 to 300 s (inset: Photographs showing color change of reducing 4-NP to 4-AP). b) Plot of $\ln(C_t/C_0)$ as a function of time obtained from part (a). c) Plot of $\ln(C_t/C_0)$ versus time for reducing 4-NP from 0 to 240 s in the presence of BP-Au synthesized from $HAuCl_4$ with different concentrations. d) Plot of $\ln(C_t/C_0)$ versus time for reducing 4-NP in the presence of Au NPs, FL-BP, simple mixing of two components (FL-BP + Au NPs), BP-Au, and RGO-Au, respectively. e) A schematic showing the enhanced catalytic activity toward 4-NP reduction by Au with FL-BP as a 2D electron reservoir.

(Figures S16c,d and S17, Supporting Information), small Au NPs and intact FL-BP nanosheets work together to achieve the highest catalytic activity ($k = 8.7 \times 10^{-3}$ s^{-1}). Therefore, the optimal concentration of $HAuCl_4$ is 0.1×10^{-3} M. Figure 3d compares the catalytic activity of FL-BP, Au NPs, simple mixing of two components (FL-BP + Au NPs), BP-Au, and RGO-Au. The concentration of Au NPs was calculated by the Au loading amount of 7.2%; the concentrations of FL-BP and RGO were kept at 0.05 mg mL^{-1}. Obviously, the k value of BP-Au is higher (11.8×10^{-3} s^{-1}) than that of addition of two components alone or simple mixing of two components (0.7×10^{-3} s^{-1}). Interestingly, the k value for BP-Au is even higher than RGO-Au (11.8×10^{-3} vs 2.9×10^{-3} s^{-1}), indicating that BP-Au has a higher catalytic activity than RGO-Au.

Figure 4 shows the TEM image, XPS spectra, and zeta potentials of BP-Au before and after reducing 4-NP. The TEM image shows that the nanosheet structure of FL-BP in BP-Au was collapsed after the catalytic reaction (Figure 4a,d). XPS spectra show that the FL-BP in BP-Au is further oxidized to be P_xO_y species (Figure 4b,e). Zeta potential decreases from –40.1 to –47.8 mV (Figure 4c,f) after the reaction. All the above results demonstrate that the FL-BP in BP-Au is oxidized during catalytic reduction of 4-NP. Therefore, the electron-reservoir and electron-donor properties of FL-BP are advantages here to enhance the catalytic activity for reducing 4-NP. Figure 3e shows a scheme illustrating enhanced catalytic activity toward 4-NP reduction by Au NPs with FL-BP as an electron donor and as a 2D electron reservoir. During this reaction, 4-NP is the electron acceptor, Au NPs is the catalyst and electron transporter, FL-BP is oxidized to release electrons and serves as an electron reservoir and an electron transporter. Therefore, FL-BP could act as an electron reservoir and an electron donor to boost the catalytic activity for reducing 4-NP.

2.2.2. Adsorption of Anti-CEA Inhibiting Catalytic Activity

Based on the excellent catalytic activity, BP-Au could be applied for detecting cancer biomarker. Before adsorbing antibody, BP-Au could reduce yellow 4-NP to colorless 4-NP

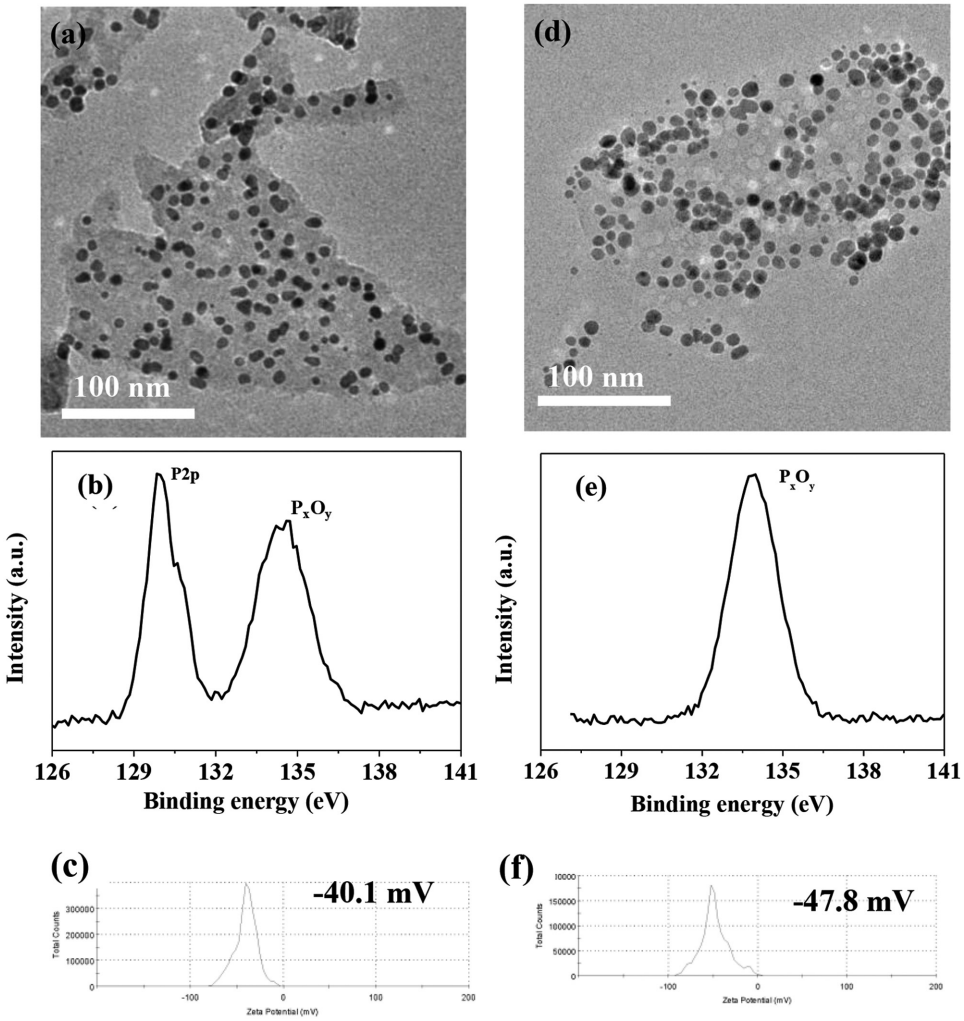

Figure 4. TEM images, XPS spectra, and zeta potentials of BP-Au a–c) before and d–f) after catalyzing 4-NP reduction.

(**Figure 5**b, inset). However, after adsorbing anti-CEA, the catalytic activity of BP-Au dropped to 1.98%, and yellow 4-NP could still be observed (Figure 5a,b). Inhibited catalytic activity of BP-Au upon anti-CEA adsorption was further supported by UV–vis spectra (Figure S18a,b, Supporting Information). This result indicates that the catalytic activity of BP-Au decreases with the increasing concentration of anti-CEA, and the optimal concentration of anti-CEA is 10 μg mL^{-1} (Figure S19, Supporting Information).

2.2.3. Detection of CEA Protein in Phosphate Buffered Saline Buffer

Clinically, the CEA test is often used for the diagnosis, prognosis, and monitoring of colon cancer, breast cancer, and lung cancer. Usually, the concentration of the biomarker secreted to the blood stream by tumors in their early stages of growth is very low.[18] Therefore, it remains a challenge to develop a sensitive method to detect the biomarker. Here, the catalytic activity of BP-Au–anti-CEA was restored after adding target antigen-CEA; yellow 4-NP could be reduced to colorless 4-AP; and the catalytic activity could be controlled by CEA concentration (C_{CEA}; Figure 5c; Figure S20c,d, Supporting Information). Therefore, the proposed colorimetric method could be used to detect CEA. The linear range for CEA detection in phosphate buffered saline (PBS) buffer is from 1 pg mL^{-1} to 10 μg mL^{-1} ($(C_0 - C_t)/C_0 = 0.10 \log C_{CEA} + 1.27$, $R^2 = 0.9902$) with a detection limit of 0.20 pg mL^{-1} (signal-to-noise ratio (S/N) is 3), which is lower than that of RGO-Au (100 pg mL^{-1}; Figures S21 and 22, Supporting Information) and other biosensors (**Table 1**).

2.2.4. Detection of CEA in Diluted Human Serum

To further investigate the selectivity and anti-interference ability of the biosensor, the detection of CEA protein in medium of diluted human serum was carried out as there were many other proteins (e.g., albumin and immunoglobulins) in human serum (**Figure 6**a,b). According to the calibration curve, two separate linear ranges for CEA detection in diluted serum medium are from 1 to 10^4 ng mL^{-1} ($(C_0 - C_t)/C_0 = 0.1759 \log C_{CEA} + 1.7025$, $R^2 = 0.9933$) and from 0.01 to 1 ng mL^{-1} ($(C_0 - C_t)/C_0 = 0.0510 \log C_{CEA} + 0.5909$, $R^2 = 0.9998$) with a detection limit of 11.5 pg mL^{-1} (S/N = 3), which fully

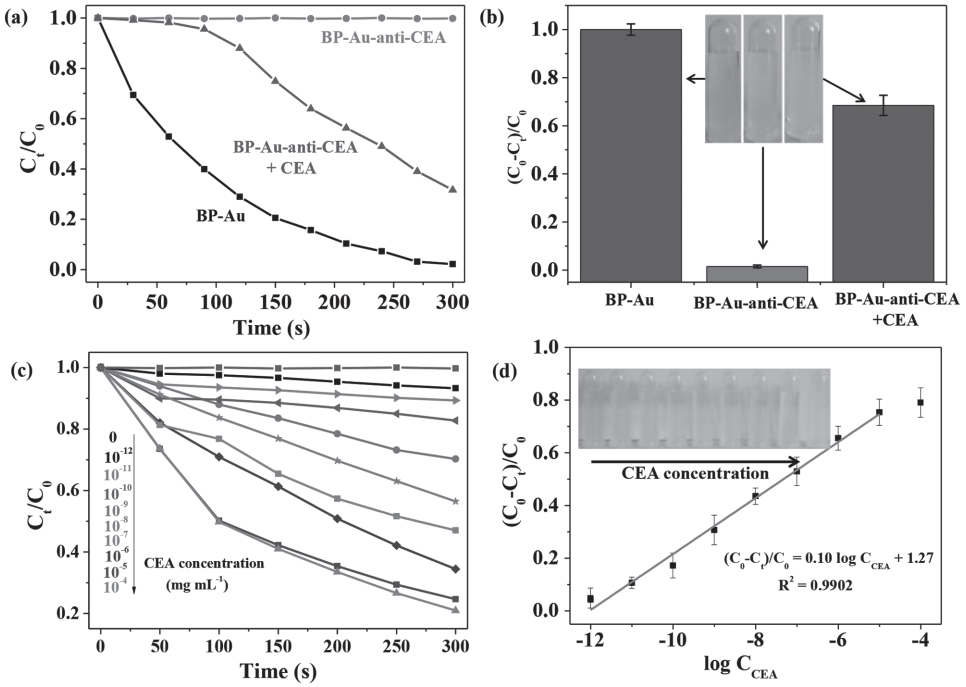

Figure 5. a) Plot of C_t/C_0 against time in reducing 4-NP by different catalysts. b) $(C_0 - C_t)/C_0$ values and optical photographs (inset) of the above three products at 300 s. c) Plot of C_t/C_0 against the reaction time in reducing 4-NP over BP-Au–anti-CEA in the presence of CEA with different concentrations. d) The calibration plot shows a good linear relationship between the $(C_0 - C_t)/C_0$ and the logarithm values of CEA concentrations (C_{CEA}) in 10×10^{-3} M PBS buffer. Inset: Optical photographs of reducing products in the presence of CEA with different concentrations. Data are the mean ± standard deviation of three different experiments.

satisfies the requirement for real clinical test (0–2.5 ng mL^{-1} for normal person and 5 to over 1000 ng mL^{-1} for patients).[21] Proteins, such as bovine serum albumin (BSA), prostate-specific antigen (PSA), and alpha fetoprotein (AFP), were further used to investigate the selectivity of this biosensing system. Figure 6c shows that the $(C_0 - C_t)/C_0$ values of these interfering proteins (10 µg mL^{-1}) were negligible compared with that of CEA (1 µg mL^{-1}). This indicates that this biosensing system has a high selectivity for CEA, which is attributed to the high affinity of anti-CEA and CEA. Moreover, BP-Au could be used to detect CEA for five times (Figure 6d), though the $(C_0 - C_t)/C_0$ value decreased every time, resulting from the inhibited catalytic of BP-Au by some adsorbed anti-CEA and CEA complexes on the surface of BP-Au.

2.3. Detection Mechanism

As strong noncovalent binding of protein and Au NPs by hydrophobic interaction and van der Waals force were

Table 1. Sensitivity of nanomaterial-based immunosensors for detecting cancer biomarkers.

Sensing element	Biomarker	Transducer	Linear range [ng mL^{-1}]	Detection limit [ng mL^{-1}]	Ref.
Nano-Au/chitosan composite	CEA	Amperometric	0.2–120.0	0.06	[19a]
Carbon-nanotube-based film decorated with Au nanoclusters	CEA	Amperometric	0.1–2 and 2–160	0.06	[19b]
Au NP–anti-CEA–HRP	CEA	Colorimetric	0.05–50	0.048	[19c]
Ag@Au core–shell NPs	CEA	DLS	0.06–50	0.0356	[19d]
$ZnFe_2O_4$–multiwalled carbon nanotubes	CEA	Colorimetric	0.005–30	0.0026	[19e]
Graphene nanocomposites	CEA	Electrochemical	0.5–60	0.1	[19f]
Magnetic microparticles	CEA	Colorimetric	2–40	0.02	[19g]
Paper-based microfluidic electrochemical immunodevice	CEA	Electrochemical	0.01–100	0.01	[19h]
Magnetic bead	PSA	Colorimetric	0.05–20	0.03	[20a]
Graphene oxide	PSA	Colorimetric	0.1–10	0.1	[20b]
Palladium nanostructures	PSA	Colorimetric	0.1–20	0.05	[20c]
DNAzyme-functionalized Au NPs	AFP	Colorimetric	0.2–20	0.1	[20d]
BP-Au	CEA	Colorimetric	0.001–10 000	0.0002	This work

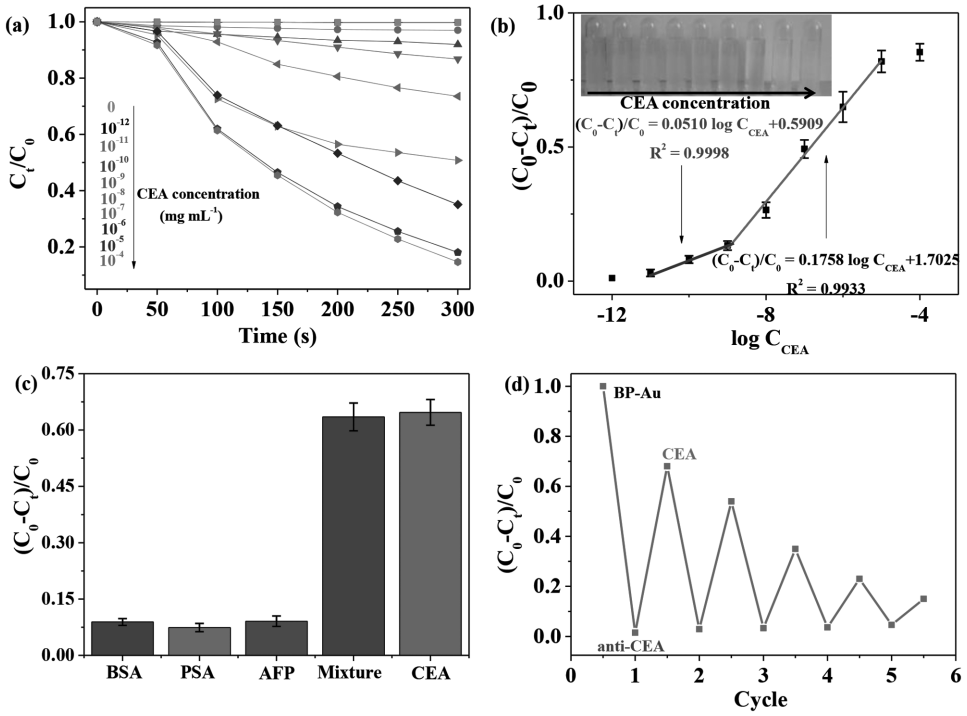

Figure 6. a) Plot of C_t/C_0 against the reaction time in reducing 4-NP over BP-Au–anti-CEA in the presence of CEA with different concentrations in diluted human serum. b) The calibration plot shows two good linear relationships between $(C_0 - C_t)/C_0$ and the logarithm value of C_{CEA} in serum. Inset: Photographs of reducing products in the presence of CEA with different concentrations. c) Selectivity of BP-Au–anti-CEA in BSA, PSA, AFP, CEA, and the mixture of these four proteins. d) The repeatability of the biosensing system. $(C_0 - C_t)/C_0$ values for anti-CEA adsorption and CEA detection for five times. Data are the mean ± standard deviation of three different experiments.

reported,[22] and there is an electrostatic repulsion between negatively charged FL-BP and anti-CEA (isoelectric point: 5.2), we anticipated that Au NPs would adsorb anti-CEA and completely inhibited the catalytic activity of BP-Au toward 4-NP reduction. In the presence of a target CEA protein, added CEA would bind with anti-CEA to form antigen–antibody complex in solution, shifting the equilibrium to desorb the anti-CEA from surface of BP-Au, which in turn "switched on" the catalytic reaction. At the same time, the hydrophobic groups of antigen–antibody complex would be packed inside forming hydrophobic clusters, and the hydrophilic groups would present on the surface, thus decreasing the hydrophobic interaction and van der Waals force between the antigen–antibody complex and Au NPs to release the antigen–antibody complex to solution, resulting in restoration of catalytic activity toward 4-NP reduction (Scheme 1). To further support our speculation, Nyquist diagrams of anti-CEA-conjugated BP-Au (BP-Au–anti-CEA) before and after adsorbing CEA were collected (**Figure 7**a). Before adsorbing anti-CEA, BP-Au-modified glass-carbon electrode (GCE/BP-Au) showed good conductivity, and the electron transfer resistance (R_{ct}) was 342 Ω compared to GCE (R_{ct} = 257 Ω). After adsorbing anti-CEA, the conductivity decreased and R_{ct} increased from 342 to 742 Ω, indicating that the anti-CEA had been successfully adsorbed on BP-Au. Notably, after the BP-Au–anti-CEA further incubating with target CEA protein, the conductivity increased and R_{ct} decreased from 742 to 601 Ω, indicating that the formed antigen–antibody complex of CEA and anti-CEA had changed conformation or a part of complex had been released from the BP-Au surface (Figure 7b). To further confirm the above results, during every step, the immune response was measured by standard bicinchoninic acid (BCA) Protein Assay Kit (Product No. P0009). As shown in Figure 7c, the added anti-CEA was 103 μg mL^{-1}. Anti-CEA adsorbed on BP-Au was 19 μg mL^{-1} and the free anti-CEA in solution was 84 μg mL^{-1}, which was in accordance with the calculated result (103 = 19 + 84). Subsequently, after adding 11 μg mL^{-1} of CEA protein, the protein on BP-Au was decreased from 19 to 10 μg mL^{-1}, and the released antigen–antibody complex and free CEA in solution were 20 μg mL^{-1}, which was also consistent with the calculated result (19 + 11 = 10 + 20). This indicates that a part of antigen–antibody complex has been released to solution. To further quantify the adsorbing and desorbing amounts of proteins, BP-Au-coated silicon wafer was hung on a microbalance and the weight was real-time monitored (Figure 7d). After adding anti-CEA, the weight increased gradually with time and reached an equilibrium after 25 min, and 0.18 mg of anti-CEA was adsorbed on BP-Au. Then, free anti-CEA was removed and BP-Au-coated silicon wafer was further immersed in CEA solution (20 μg mL^{-1}). The weight decreased gradually with time and reached an equilibrium after 15 min, and 0.04 mg of antigen–antibody complex was released from the surface of BP-Au. Therefore, the above results further support our suggested detection mechanism.

2.4. Detection of CEA in Real Clinical Samples

Enzyme-linked immunosorbent assay (ELISA) has been the gold standard for protein concentration determination.[23]

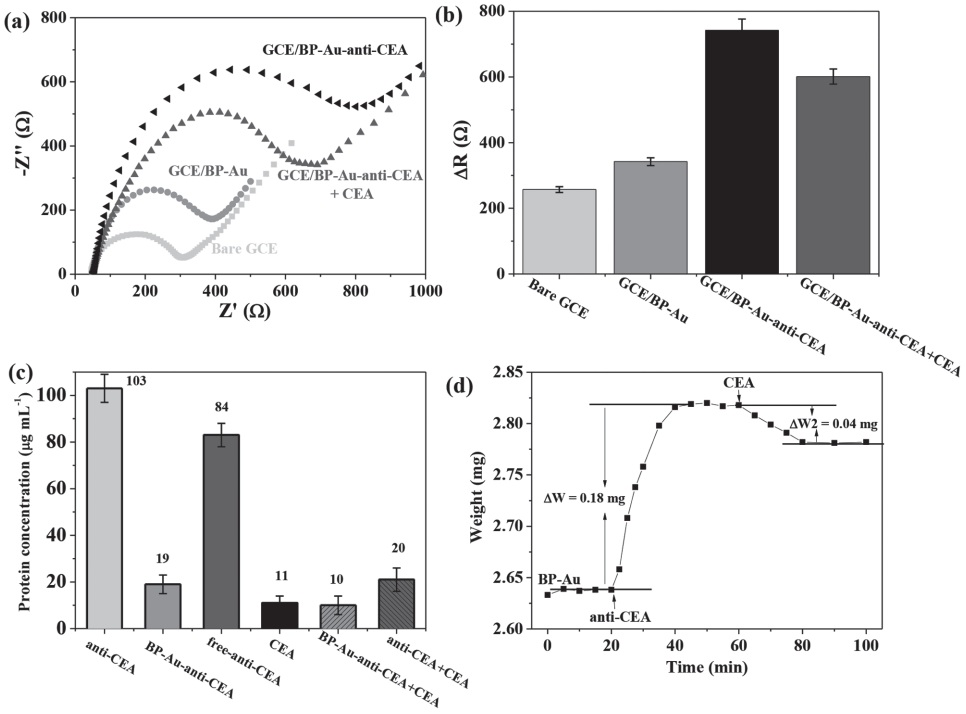

Figure 7. a) Nyquist diagrams of bare GCE, BP-Au-modified-GCE, BP-Au–anti-CEA-modified GCE before and after incubation with 1 μg mL^{-1} CEA. b) Δ*R* of GCE and the modified GCEs. c) Protein amounts of added anti-CEA, anti-CEA immobilized on BP-Au (BP-Au–anti-CEA), free anti-CEA in solution, added CEA, antigen–antibody complex adsorbed on BP-Au after immune reaction (BP-Au–anti-CEA + CEA), antigen–antibody complex desorbed from BP-Au surface (anti-CEA + CEA) measured by BCA Protein Assay Kit. d) Weight with time was measured for BP-Au-coated silicon slice which was immersed in PBS buffer. Then, anti-CEA (100 μg mL^{-1}) was added at 20 min and CEA (20 μg mL^{-1}) was added at 60 min, respectively.

To investigate the application of our biosensing system in the clinical test, eight human serum samples (four colon cancer patients and four breast cancer patients) were provided by the First Affiliated Hospital of Xiamen University. The concentrations of CEA in these samples were 100.00, 57.56, 6.92, 4.49, 7.12, 6.27, 6.29, and 7.17 ng mL^{-1} measured by the ELISA method, respectively. The corresponding concentrations of CEA measured by our proposed method were 104.19, 55.93, 7.08, 4.33, 6.95, 6.36, 6.44, and 7.29 ng mL^{-1}, respectively (**Figure 8**). The recovery for eight clinical samples was in the range from 96.44% to 104.19% (Table S3, Supporting Information). The results indicate that the assay can be applied in the clinical diagnosis of colon and breast cancers. Therefore, the stability-related limitation of FL-BP can also be the advantage for application in detecting cancer biomarker in clinic.

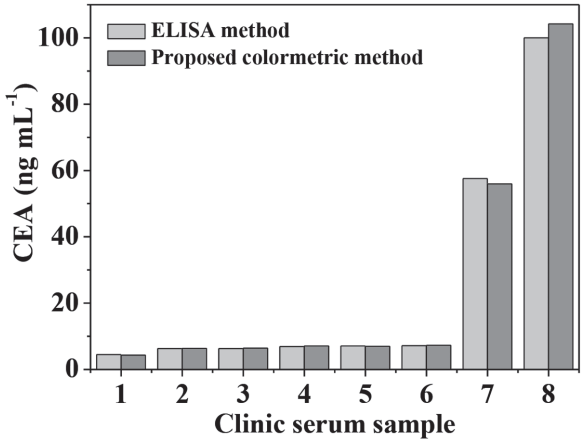

Figure 8. The concentration of CEA in clinical serum samples determined by our and standard ELISA methods.

3. Conclusion

In conclusion, the instability- or stability-related limitation of BP was used for enhancing catalytic activity and constructing colorimetric biosensor for the first time. BP-Au hybrid was prepared by simply mixing Au precursor with as-synthesized FL-BP at room temperature for a few minutes. The obtained hybrid exhibited promising catalytic activity in reducing 4-NP (K = 1120 s^{-1} g^{-1}, E_a = 17.53 kJ mol^{-1}). Catalytic activity of the obtained BP-Au became "inactive" by treating with antibody, and reversibly turned to "active" upon treatment with corresponding antigen in solution, thus providing a powerful and versatile method for label-free colorimetric detection of biomarker. This colorimetric sensor had a low detection (0.20 pg mL^{-1}) and wide linear range (1 pg mL^{-1} to 10 μg mL^{-1}), and was used to detect clinical samples.

4. Experimental Section

Preparation of FL-BP: Bulk BP was prepared according to the literature.[13] FL-BP was prepared by liquid exfoliation of corresponding bulk BP in PVP solution. In detail, 20 mg of as-obtained bulk BP was dispersed in a 50 mL centrifugal tube containing

40 mL of stock solution of PVP (0.50 mg mL^{-1}) that bubbled with argon to eliminate the dissolved oxygen molecules for avoiding the oxidation, and its lid was sealed with polydimethylsiloxane several times to occlude O_2 and H_2O. Then the mixture solution was sonicated in ice water for 30 h. Afterward, the resultant brown suspension was centrifuged at 1000 rpm for 20 min to remove the residual unexfoliated BP and the supernatant was centrifuged at 12 000 rpm for 20 min to remove free PVP, and the precipitate was collected for further use. Exfoliated FL-BP in H_2O (FL-BP/H_2O) was prepared by the similar method of FL-BP except that PVP was replaced by pure water.

Preparation of BP-Au: After 1 mL of FL-BP suspension (0.25 mg mL^{-1}) was centrifuged at 12 000 rpm for 20 min, the supernatant was removed and the precipitate was redispersed in 4 mL of aqueous solution containing 0.3×10^{-3} M sodium citrate (SC). 50 µL of $HAuCl_4$ aqueous solution (10×10^{-3} M) was added into this solution with mild shaking. Within 5 min, the solution color was turned from brown to purple, indicating the production of BP-Au. The resulting solution was then centrifuged at 10 000 rpm for 20 min, and the precipitate was redispersed in water before further characterization. Note that without SC, the deposition of Au NPs on FL-BP nanosheets could also occur. In our synthesis, the SC served as a surface capping agent for the better dispersion of the BP-Au hybrid nanomaterials in water. Au-NP-loaded reduced RGO-Au was prepared according to our previous report.[24]

Catalytic Reduction of 4-NP: Aqueous solution of $NaBH_4$ (0.42 M, 10 mL) was added to 4-NP aqueous solution (0.175×10^{-3} M, 70 mL) at room temperature. Then 50 µL of BP-Au suspension (0.25 mg mL^{-1}) was mixed with 3 mL of 4-NP aqueous solution at room temperature for measuring the UV–vis spectra at same intervals.

Preparation of BP-Au–Anti-CEA: 50 µL of BP-Au suspension (0.1 mg mL^{-1}) was mixed with 50 µL of anti-CEA (0.1 mg mL^{-1}) in 10×10^{-3} M PBS buffer (pH 7.4) and incubated for 10 min to form BP-Au–anti-CEA. The suspension was centrifuged at 10 000 rpm for 5 min to remove free anti-CEA, and the precipitate was redispersed in water and stored at 4 °C before use. For inhibiting catalytic assay, the purified BP-Au–anti-CEA suspension was then added to 1 mL of 4-NP aqueous solution at room temperature, and UV–vis spectra at same intervals were measured.

Confirming Desorption of CEA Antigen–Antibody Complex—Electrochemical Impedance Spectroscopy (EIS): 10 µL of BP-Au (0.1 mg mL^{-1}) was dropped onto the GCE to prepare GCE/BP-Au. GCE/BP-Au–anti-CEA was obtained by immersing GCE/BP-Au in PBS buffer containing anti-CEA (0.01 mg mL^{-1}) for 10 min, and then rinsed with PBS for 30 s to remove unattached anti-CEA. For immune reaction, GCE/BP-Au–anti-CEA was immersed in PBS containing CEA (0.01 mg mL^{-1}) for 10 min, and then rinsed with PBS for 30 s to remove excess CEA. EIS measurements of GCE/BP-Au, GCE/BP-Au–anti-CEA, and GCE/BP-Au–anti-CEA + CEA were performed, respectively. The EIS was performed in 5.0×10^{-3} M $[Fe(CN)_6]^{3-/4-}$ and 1.0 M KCl solution. The AC voltage amplitude was 5 mV and the voltage frequencies ranged from 0.1 to 10^5 Hz.

Real-time weight measurements were performed on a microbalance (KSV NIMA). Silicon wafer was washed successively with 1:1 nitric acid, ethanol, and doubly distilled water in an ultrasonic bath and dried in air. 50 µL of BP-Au (0.1 mg mL^{-1}) dispersion was dropped onto silicon wafer to prepare BP-Au-coated silicon wafer. Then, the modified silicon wafer was dried naturally overnight. To quantify the adsorbing quantity of anti-CEA, the modified wafer was immersed in PBS buffer containing 0.1 mg mL^{-1} anti-CEA. The modified wafer was hung on a microbalance and the weight was real-time monitored. To confirm the release of antigen–antibody complex, PBS buffer containing free antibody was replaced by PBS buffer containing 0.02 mg mL^{-1} CEA; BP-Au-coated silicon wafer was hung on a microbalance and the weight was real-time monitored.

Samples for Enhanced BCA Protein Assay Kit: 50 µL of BP-Au suspension (0.1 mg mL^{-1}) was mixed with 50 µL of anti-CEA (0.1 mg mL^{-1}) in 10×10^{-3} M PBS buffer (pH = 7.4) and incubated for 10 min to form BP-Au–anti-CEA. The suspension was centrifuged at 10 000 rpm for 5 min to collect free anti-CEA and precipitate, respectively. The precipitate (BP-Au–anti-CEA) was redispersed in water. 50 µL of CEA biomarker aqueous solution (0.01 mg mL^{-1}) was incubated with the above BP-Au–anti-CEA in 10×10^{-3} M PBS buffer for 10 min for immune reaction. The suspension was centrifuged at 10 000 rpm for 5 min to collect free antigen–antibody complex and precipitate, respectively. The added anti-CEA, CEA protein, and collected samples were used for protein content measurement by enhanced BCA Protein Assay Kit.

Label-Free Colorimetric Detection of Cancer Marker (CEA)—Label-Free Colorimetric Detection of CEA in PBS Buffer: 50 µL of CEA biomarker aqueous solution (in desired concentration) was incubated with above BP-Au–anti-CEA in 10×10^{-3} M PBS buffer for 10 min. The solution was transferred to 4-NP (0.175×10^{-3} M, 1 mL) aqueous solution at room temperature, and the time-dependent absorbance measurements were then recorded.

Label-Free Colorimetric Detection of Cancer Marker (CEA)—Label-Free Colorimetric Detection of CEA in Diluted Serum: 50 µL of CEA (in desired concentration) aqueous solution was incubated with 50 µL of BP-Au–anti-CEA (0.1 mg mL^{-1}) in 1% serum of normal persons for 10 min. The solution was then transferred to 4-NP (0.175×10^{-3} M, 1 mL) aqueous solution at room temperature, and the time-dependent absorbance measurements were then recorded.

Label-Free Colorimetric Detection of Cancer Marker (CEA)—Label-Free Colorimetric Detection of Undiluted Serum from Colon Patients: 50 µL of undiluted serum from colon patients of the First Affiliated Hospital of Xiamen University was incubated with 50 µL of BP-Au–anti-CEA (0.1 mg mL^{-1}) for 10 min. The solution was then transferred to 4-NP (0.175×10^{-3} M, 1 mL) aqueous solution at room temperature, and the time-dependent absorbance measurements were then recorded.

Supporting Information

Supporting Information is available from the Wiley Online Library or from the author.

Acknowledgements

J.P. and Y.Q.L. contributed equally to this work. This work was supported by the National Key Scientific Research Projects

(Grant No. 2014CB932004), National Natural Science Foundation of China (Grant Nos. 31371005 and 81171453), "111" Project (Grant No. B16029), and Scientific and Technological Innovation Platform of Fujian Province of China (Grant No. 2014H2006).

[1] J. Sun, G. Y. Zheng, H. W. Lee, N. Liu, H. T. Wang, H. B. Yao, W. S. Yang, Y. Cui, *Nano Lett.* **2014**, *14*, 4573.

[2] a) E. S. Reich, *Nature* **2014**, *506*, 19; b) A. Favron, E. Gaufres, F. Fossard, A. L. Phaneuf-L'Heureux, N. Y. W. Tang, P. L. Levesque, A. Loiseau, R. Leonelli, S. Francoeur, R. Martel, *Nat. Mater.* **2015**, *14*, 826; c) V. Eswaraiah, Q. S. Zeng, Y. Long, Z. Liu, *Small* **2016**, *12*, 3480; d) S. Balendhran, S. Walia, H. Nili, S. Sriram, M. Bhaskaran, *Small* **2015**, *11*, 640; e) L. K. Li, Y. J. Yu, G. J. Ye, Q. Q. Ge, X. D. Ou, H. Wu, D. L. Feng, X. H. Chen, Y. B. Zhang, *Nat. Nanotechnol.* **2014**, *9*, 372; f) H. R. Wu, X. F. Liu, J. Yin, J. X. Zhou, W. L. Guo, *Small* **2016**, *12*, 5276; g) N. N. Mao, J. X. Wu, B. Han, J. J. Lin, L. M. Tong, J. Zhang, *Small* **2016**, *12*, 2627; h) Y. J. Xu, J. Yuan, L. F. Fei, X. L. Wang, Q. L. Bao, Y. Wang, K. Zhang, Y. G. Zhang, *Small* **2016**, *12*, 5000.

[3] H. Liu, A. T. Neal, Z. Zhu, Z. Luo, X. F. Xu, D. Tomanek, P. D. D. Ye, *ACS Nano* **2014**, *8*, 4033.

[4] a) F. N. Xia, H. Wang, Y. C. Jia, *Nat. Commun.* **2014**, *5*, 4458; b) M. Buscema, D. J. Groenendijk, S. I. Blanter, G. A. Steele, H. S. J. van der Zant, A. Castellanos-Gomez, *Nano Lett.* **2014**, *14*, 3347; c) J. S. Qiao, X. H. Kong, Z. X. Hu, F. Yang, W. Ji, *Nat. Commun.* **2014**, *5*, 4475.

[5] a) L. Z. Kou, T. Frauenheim, C. F. Chen, *J. Phys. Chem. Lett.* **2014**, *5*, 2675; b) L. Tony, E. Michael, S. Mathias, A. Phaedon, *Phys. Rev. B* **2014**, *90*, 081408.

[6] a) R. A. Doganov, E. C. T. O'Farrell, S. P. Koenig, Y. T. Yeo, A. Ziletti, A. Carvalho, D. K. Campbell, D. F. Coker, K. Watanabe, T. Taniguchi, A. H. C. Neto, B. Ozyilmaz, *Nat. Commun.* **2015**, *6*, 6647; b) Q. Zhou, Q. Chen, Y. Tong, J. Wang, *Angew. Chem., Int. Ed.* **2016**, *55*, 11437; c) J. S. Kim, Y. N. Liu, W. N. Zhu, S. Kim, D. Wu, L. Tao, A. Dodabalapur, K. Lai, D. Akinwande, *Sci. Rep.* **2015**, *5*, 8989; d) A. Avsar, I. J. Vera-Marun, J. Y. Tan, K. Watanabe, T. Taniguchi, A. H. C. Neto, B. Ozyilmaz, *ACS Nano* **2015**, *9*, 4138.

[7] a) C. R. Ryder, J. D. Wood, S. A. Wells, Y. Yang, D. Jariwala, T. J. Marks, G. C. Schatz, M. C. Hersam, *Nat. Chem.* **2016**, *8*, 597; b) Y. Zhao, H. Wang, H. Huang, Q. Xiao, Y. Xu, Z. Guo, H. Xie, J. Shao, Z. Sun, W. Han, X. F. Yu, P. Li, P. K. Chu, *Angew. Chem., Int. Ed.* **2016**, *55*, 5003; c) J. J. Pei, X. Gai, J. Yang, X. B. Wang, Z. F. Yu, D. Y. Choi, B. L. Davies, Y. R. Lu, *Nat. Commun.* **2016**, *7*, 10450; d) D. Hanlon, C. Backes, E. Doherty, C. S. Cucinotta, N. C. Berner, C. Boland, K. Lee, A. Harvey, P. Lynch, Z. Gholamvand, S. F. Zhang, K. P. Wang, G. Moynihan, A. Pokle, Q. M. Ramasse, N. McEvoy, W. J. Blau, J. Wang, G. Abellan, F. Hauke, A. Hirsch, S. Sanvito, D. D. O'Regan, G. S. Duesberg, V. Nicolosi, J. N. Coleman, *Nat. Commun.* **2015**, *6*, 8563.

[8] Z. Sofer, D. Sedmidubsky, S. Huber, J. Luxa, D. Bousa, C. Boothroyd, M. Pumera, *Angew. Chem., Int. Ed.* **2016**, *55*, 3382.

[9] R. Xu, J. Yang, Y. Zhu, H. Yan, J. Pei, Y. W. Myint, S. Zhang, Y. Lu, *Nanoscale* **2016**, *8*, 129.

[10] a) H. Wang, X. Z. Yang, W. Shao, S. C. Chen, J. F. Xie, X. D. Zhang, J. Wang, Y. Xie, *J. Am. Chem. Soc.* **2015**, *137*, 11376; b) X. Ling, H. Wang, S. X. Huang, F. N. Xia, M. S. Dresselhaus, *Proc. Natl Acad. Sci. USA* **2015**, *112*, 4523; c) Z. B. Sun, H. H. Xie, S. Y. Tang, X. F. Yu, Z. N. Guo, J. D. Shao, H. Zhang, H. Huang, H. Y. Wang, P. K. Chu, *Angew. Chem., Int. Ed.* **2015**, *54*, 11526.

[11] a) H. U. Lee, S. Y. Park, S. C. Lee, S. Choi, S. Seo, H. Kim, J. Won, K. Choi, K. S. Kang, H. G. Park, H. S. Kim, H. R. An, K. H. Jeong, Y. C. Lee, *Small* **2016**, *12*, 214; b) C. Dissanayake, *Science* **2005**, *309*, 883.

[12] a) H. U. Lee, S. Y. Park, S. C. Lee, S. Choi, S. Seo, H. Kim, J. Won, K. Choi, K. S. Kang, H. G. Park, H. S. Kim, H. R. An, K. H. Jeong, Y. C. Lee, *Small* **2016**, *12*, 214; b) C. Sun, L. Wen, J. Zeng, Y. Wang, Q. Sun, L. Deng, C. Zhao, Z. Li, *Biomaterials* **2016**, *91*, 81; c) S. Yan, B. Wang, Z. Wang, D. Hu, X. Xu, J. Wang, Y. Shi, *Biosens. Bioelectron.* **2016**, *80*, 34.

[13] M. C. Stan, J. von Zamory, S. Passerini, T. Nilges, M. Winter, *J. Mater. Chem. A* **2013**, *1*, 5293.

[14] a) Z. N. Guo, H. Zhang, S. B. Lu, Z. T. Wang, S. Y. Tang, J. D. Shao, Z. B. Sun, H. H. Xie, H. Y. Wang, X. F. Yu, P. K. Chu, *Adv. Funct. Mater.* **2015**, *25*, 6996; b) L. Chen, G. M. Zhou, Z. B. Liu, X. M. Ma, J. Chen, Z. Y. Zhang, X. L. Ma, F. Li, H. M. Cheng, W. C. Ren, *Adv. Mater.* **2016**, *28*, 510.

[15] a) R. Si, M. Flytzani-Stephanopoulos, *Angew. Chem., Int. Ed.* **2008**, *47*, 2884; b) T. Kong, J. Zeng, X. P. Wang, X. Y. Yang, J. Yang, S. McQuarrie, A. McEwanL, W. Roa, J. Chen, J. Z. Xing, *Small* **2008**, *4*, 1537.

[16] Y. Cai, G. Zhang, Y. W. Zhang, *Sci. Rep.* **2014**, *4*, 6677.

[17] M. Batmunkh, C. J. Shearer, M. J. Biggs, J. G. Shapter, *J. Mater. Chem. A* **2016**, *4*, 2605.

[18] P. M. Kosaka, V. Pini, J. J. Ruz, R. A. da Silva, M. U. Gonzalez, D. Ramos, M. Calleja, J. Tamayo, *Nat. Nanotechnol.* **2014**, *9*, 1047.

[19] a) X. L. He, R. Yuan, Y. Q. Chai, Y. T. Shi, *J. Biochem. Biophys. Methods* **2008**, *70*, 823; b) X. Gao, Y. M. Zhang, H. Chen, Z. C. Chen, X. F. Lin, *Anal. Biochem.* **2011**, *414*, 70; c) M. Liu, C. Jia, Q. Jin, X. Lou, S. Yao, J. Xiang, J. Zhao, *Talanta* **2010**, *81*, 1625; d) X. M. Miao, S. Y. Zou, H. Zhang, L. S. Ling, *Sens. Actuators, B* **2014**, *191*, 396; e) W. Y. Liu, H. M. Yang, Y. A. Ding, S. G. Ge, J. H. Yu, M. Yan, X. R. Song, *Analyst* **2014**, *139*, 251; f) X. Chen, X. L. Jia, J. M. Han, J. Ma, Z. F. Ma, *Biosens. Bioelectron.* **2013**, *50*, 356; g) J. Wang, Y. Cao, Y. Y. Xu, G. X. Li, *Biosens. Bioelectron.* **2009**, *25*, 532; h) Y. F. Wu, P. Xue, K. M. Hui, Y. J. Rang, *Biosens. Bioelectron.* **2014**, *52*, 180.

[20] a) Z. Q. Gao, M. D. Xu, L. Hou, G. N. Chen, D. P. Tang, *Anal. Chem.* **2013**, *85*, 6945; b) F. L. Qu, T. Li, M. H. Yang, *Biosens. Bioelectron.* **2011**, *26*, 3927; c) Z. Q. Gao, L. Hou, M. D. Xu, D. P. Tang, *Sci. Rep.* **2014**, *4*, 3966; d) W. H. Zhou, C. L. Zhu, C. H. Lu, X. C. Guo, F. R. Chen, H. H. Yang, X. R. Wang, *Chem. Commun.* **2009**, *44*, 6845.

[21] C. B. Wood, J. G. Ratcliffe, R. W. Burt, A. J. H. Malcolm, L. H. Blumgart, *Br. J. Surg.* **1980**, *67*, 46.

[22] a) S. H. Lacerda, J. J. Park, C. Meuse, D. Pristinski, M. L. Becker, A. Karim, J. F. Douglas, *ACS Nano* **2010**, *4*, 365; b) B. D. Chithrani, W. C. Chan, *Nano Lett.* **2007**, *7*, 1542.

[23] E. Engvall, P. Perlmann, *J. Immunol.* **1972**, *109*, 129.

[24] X. C. Lv, J. Weng, *Sci. Rep.* **2013**, *3*, 3285.

Received: October 26, 2016
Published online:

